Digest Journal of Nanomaterials and Biostructures Vol. 8, No. 2, April - June 2013, p. 667 - 675

PHOTOLUMINESCENCE AND PHOTOCATALYTIC ACTIVITY OF Mn-DOPED ZnO NANOPARTICLES

G. VOICU, O. OPREA [*], B. S. VASILE, E. ANDRONESCU
University Politehnica of Bucharest, Faculty of Applied Chemistry and Materials Science, Romania

Nanocrystalline ZnO particles doped with Mn(II) ions were prepared by a forced hydrolysis method of zinc acetate dihydrate and manganese acetate tetrahydrate, under reflux, in buthanol. The precipitate obtained was separated by centrifugation at 9.000 rpm and purified by refluxing in water. The dopant percentage was 1, 2.5 and 5%. The qualitative composition of the nanopowder has been evidenced in the elemental EDS maps. Optical investigation shows that the Mn doping in ZnO lattice leads to a decrease in the near band edge position due to the introduction of new unoccupied states by Mn *3d* electrons. The luminescence of ZnO is quenched by increasing the dopant ions percentage. At doping rate of 1% Mn in the ZnO lattice a tenfold decrease in intensity of luminescence was observed, along with modification of the luminescence pattern. Further increases of dopant percent from 1% to 5% had as result a decrease of only 30% in the luminescence intensity. The photocatalytic activity was investigated against methylene blue. The increase of Mn percentage leads to a better photocatalytic activity.

(Received March 11, 2013; Accepted April 18, 2013)

Keywords: Mn-doped zinc oxide, nanomaterials, photocatalysis

1. Introduction

In the last decade various oxide semiconductors [1-4] have been used as catalyst, phosphor, gas sensor, photocatalyst, UV-photoprotector, varistor or in dye-sensitized solar cells [5-10]. The field of applications is determined by the electrical, optical and structural properties of the semiconductors. Among them, ZnO offers some unique optoelectronic properties due to its wide bandgap of 3.3 eV and large excitonic binding energy of 60 meV.

Due to the special optical properties, high transparencies in the visible domain coupled with high absorbance of the UV radiation, ZnO has been toughly investigated as a coating material, from paints [11], to sunscreens [12] and fabric coating [13].

The photocatalytic activity of ZnO is well known and has been investigated versus a wide variety of pollutants. There are some application where a high photocatalytic activity is desirable [14], but there are also some application where ZnO capacity to degrade various organic substrate is an impediment, like f abric or paper coating.

Doping of ZnO with transition metals (TM) can lead to ferromagnetic properties at room temperature (RT FM), might form dilute magnetic semiconductors (DMSs) and is an effective way to tune the properties of ZnO [15,16]. The doping TM will create some unoccupied states that will consequently alter of the band gap energy [17]. The presence of a dopant ion in the ZnO lattice can influence also the photocatalytic capacity of the nanoparticles, in both directions, giving an easy method to tune this property to suit various applications [18-20].

In our previous works, we have prepared pure and doped ZnO by force hydrolysis, sol-gel or pyrosol methods [21-23], and we manage to tune the luminescent properties of ZnO by thermal treatment [24].

---

[*] Corresponding author: ovidiu73@yahoo.com

In the case of Mn-doped ZnO it is known that the solubility of the dopant in ZnO lattice depends on many factors (the preparation method and conditions, the annealing temperature, the doping concentration, and even the grain size). All factors are related to the structural defects that may exist in the ZnO nanoparticles, which will influence also the electronic and optoelectronic properties. The intrinsic defects commonly found in ZnO are zinc interstitials (Zn_i), zinc vacancies (V_{Zn}), oxygen interstitials (O_i), oxygen vacancies (V_O), oxygen antisites (O_{Zn}), and zinc antisites (Zn_O), as were detailed described by Kohan *et al* [25].

Samples with different Mn(II) content (1-5%) were synthesized by adapting the previously reported forced hydrolysis method in alcohol [21], from zinc acetate dihydrate and manganese acetate tetrahydrate, under reflux. The samples were structurally characterized by means UV-Vis and PL spectrometry, XRD, TEM, HRTEM and SAED. The photocatalytic activity was investigated against methylene blue.

2. Experimental procedure

Zinc acetate dihydrate, $Zn(CH_3COO)_2\cdot 2H_2O$ and $Mn(CH_3COO)_2\cdot 4H_2O$ with 99.9% purity, were obtained from Merck. Buthanol was used as received from Sigma without further purification.

2.1 Mn(II) (1%) doped ZnO synthesis

2.173g (9.9 mmoles) $Zn(CH_3COO)_2$ $2H_2O$ and 0.0245g (0.1 mmoles) $Mn(CH_3COO)_2\cdot 4H_2O$ were dissolved in 50 mL buthanol. The solution was then kept for 12h on a thermostatic bath at 120°C under magnetic stirring. The light brown colloidal precipitate formed was then separated by centrifugation at 9.000 rpm and washed several times with ethanol. The light-brown powder was dried at 105°C for 30 min in the ambient atmosphere following the removal of supernatant.

We have prepared three doped ZnO samples and a pure control sample by this method (0%, 1%, 2.5% and 5%).

2.2 Experimental techniques

a) Electron Microscope Images. The transmission electron images were obtained on ultrasonated powdered samples using a Tecnai^{TM} G^2 F30 S-TWIN high resolution transmission electron microscope from FEI, equipped with STEM/HAADF detector, EDX (Energy dispersive X-ray Analysis) and EFTEM - EELS (Electron energy loss spectroscopy) operated at an acceleration voltage of 300 KV obtained from a Shottky Field emitter with a TEM point resolution of 2 Å and line resolution of 1.02 Å.

b) X-ray Diffraction. X-ray powder diffraction patterns were obtained with a Shimadzu XRD6000 diffractometer, using Cu Kα (1.5406 Å) radiation operating with 30 mA and 40 kV in the 2θ range 10–70°. A scan rate of 1° min^{-1} was employed.

c) Photoluminescence spectra. Photoluminescence spectra (PL) were measured with a Perkin Elmer P55 spectrometer using a Xe lamp as a UV light source at ambient temperature, in the range 200-800 nm, with all the samples in solid state. The measurements were made with scan speed of 200 nm·min^{-1}, slit of 10 nm, and cut-off filter of 1% for ZnO sample and without any cut-off filter for Mn doped ZnO samples. An excitation wavelength of 320 nm was used.

d) Diffuse reflectance spectra measurements were made with a JASCO V560 spectrophotometer with solid sample accessory, in the domain 200-800nm, with a speed of 200nm·min^{-1}.

e) Photocatalytic activity was determined against methylene blue (MB) solution, 10^{-4} %, by irradiation with an Hg lamp. Samples of 0.0250 g powder were inserted in 20 mL solution of MB. Samples were allowed to stay 30 min in dark to reach the adsorption equilibrium. After that, at defined time intervals a sample of 2mL was taken out and its UV-Vis spectra was recorded.

3. Results and discussions

The figure 1 shows the XRD patterns of ZnO and Mn doped ZnO prepared by forced hydrolysis. All diffraction peaks from the samples correspond to the hexagonal ZnO structure [ASTM 80-0075]. The XRD patterns show that there was no second-phase peak and that the doping did not change the wurtzite structure of ZnO. Compared with pure ZnO, 14 nm, the crystalline particle size of Mn-doped ZnO is larger, 19.7 nm, and also its lattice parameters are larger.

The crystallite size of the samples was estimated from the Scherrer equation, $D = 0.89\cdot\lambda/\beta\cdot\cos\Theta$, where D is the average grain size, λ is the X-ray wavelength (0.15405 nm), Θ and β are the diffraction angle and FWHM of an observed peak, respectively. The strongest peak (101) was used to calculate the average crystallite size (D) of ZnO particles.

The lattice constant calculated for pure ZnO are a = b = 0.3249 nm, c = 0.5187 nm. For the Mn doped ZnO samples the values are presented in table 1. Both the 'a' and 'c' values increased slightly with the increased incorporation of Mn in the ZnO lattice as shown in table 1. Although the change is small, the concentration of the dopant plays a role in the variation in the lattice parameter, which is an indicator for the Mn doping in ZnO.

The Bragg angle of the intense (101) reflection showed a slight shift $\Delta(2\Theta_{101})$ toward smaller values relative to that of pure ZnO. This is evidence for the creation of internal compressive micro stress [26].

Table 1. Lattice parameters and the structural analysis results for the pure and Mn doped ZnO powders.

Sample	Lattice constants (nm)		$2\Theta_{(101)}$	FWHM (101)	D (nm)
	a=b	c			
ZnO	0.3249	0.5187	36.363	0.59	14.0
ZnO/ Mn 1%	0.3258	0.5193	36.358	0.48	17.2
ZnO/ Mn 2.5%	0.3261	0.5195	36.324	0.45	18.4
ZnO/ Mn 5%	0.3267	0.5196	36.319	0.42	19.7

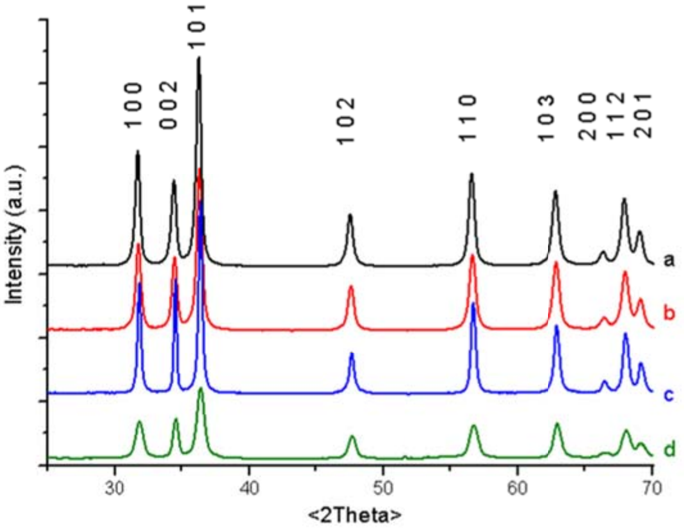

Fig. 1. XRD patterns of pure ZnO powder (d) and Mn-doped ZnO powder samples at different doping levels 1% (c), 2.5% (b) and 5% (a).

The TEM bright field image, figure 2a, of Mn-doped ZnO nanoparticles (5%) as obtained, reveals that the powder is composed from polyhedral particles, with an average size of approximately 10nm, which have a slight tendency to aggregates as nanorods with dimensions of 10nm x50 nm.

Additional information about the structures of the nanoparticles was found through detailed analysis with HRTEM. The HRTEM image, figure 2b, shows clear lattice fringes of interplanar distances of d = 1.62 Å and d = 2.59 Å/(0 0 2) for nanocrystalline ZnO, corresponding to Miller indices (1 1 0) and (0 0 2) respectively, of crystallographic planes of hexagonal ZnO. In addition, the regular succession of the atomic planes indicates that the nanocrystalites are structurally uniform and crystalline with no amorphous phase present.

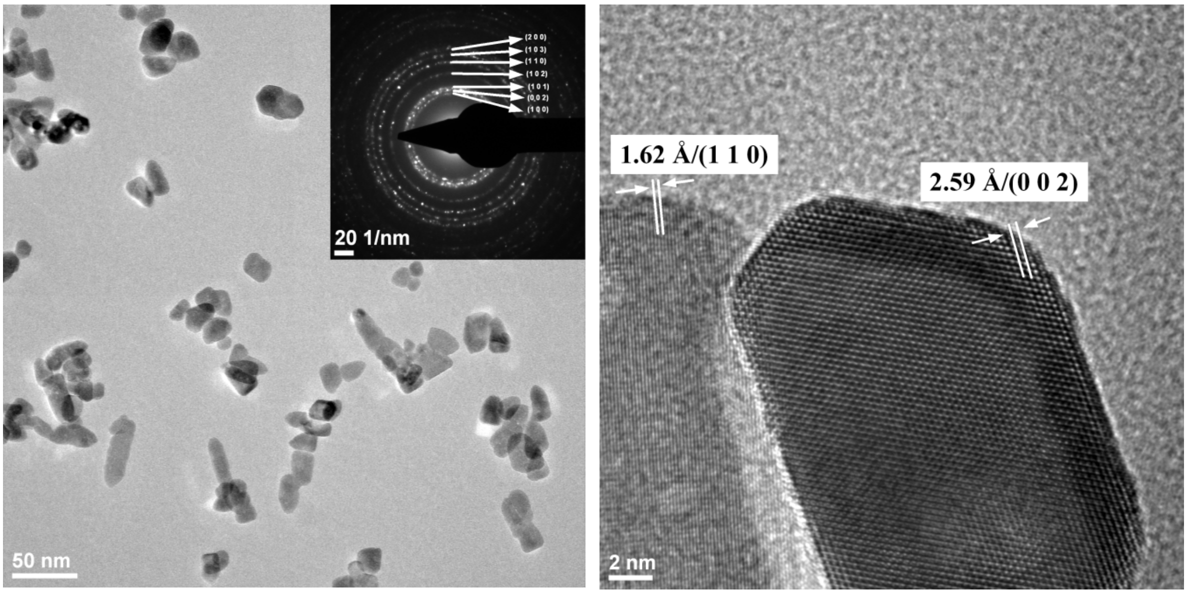

Fig. 2. (a) TEM images of 5% Mn doped ZnO polyhedral shaped particles - SAED pattern of planes of hexagonal structure ZnO [ASTM 80-0075]; (b) HRTEM with the (1 1 0) and (0 0 2) crystallographic planes of ZnO

From the selected area diffraction pattern obtained on ZnO nanopowder, we can state that the only phase identified is the crystalline hexagonal form of ZnO [ASTM 80-0075]. Moreover, the SAED image of 5% Mn doped ZnO nanoparticles confirms the Miller indices of characteristic crystalline structures identified by XRD (inset of figure 2a).

In order to correlate the microstructure and the distribution of O, Zn and Mn, qualitative analyses, e.g. elemental map and spectrum of the same region were recorded. Elemental mapping of the 5% Mn-doped sample revealed a uniform distribution of various ions in the sample (Fig.3).

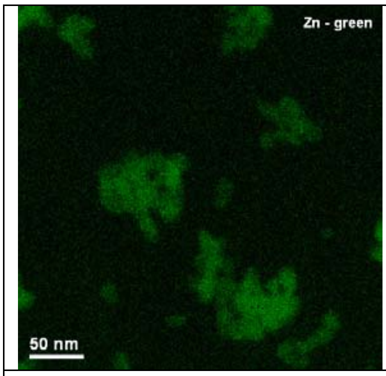	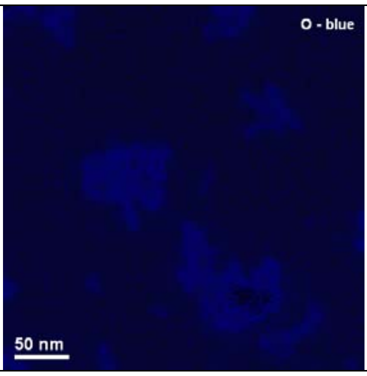	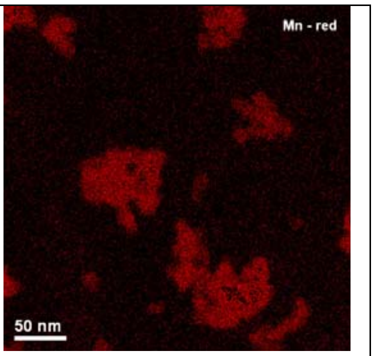
Zn	O	Mn

Fig. 3. Elemental mapping of 5%Mn-doped ZnO sample showing the presence of (a) Zn (b) O and (c) Mn ions, respectively.

The photoluminescence spectra of ZnO powders usually present two emission peaks in the UV and visible ranges [27]. The UV emission corresponds to the near band-edge emission (NBE) and the visible emission is commonly referred to as a deep-level or trap-state emission [28].

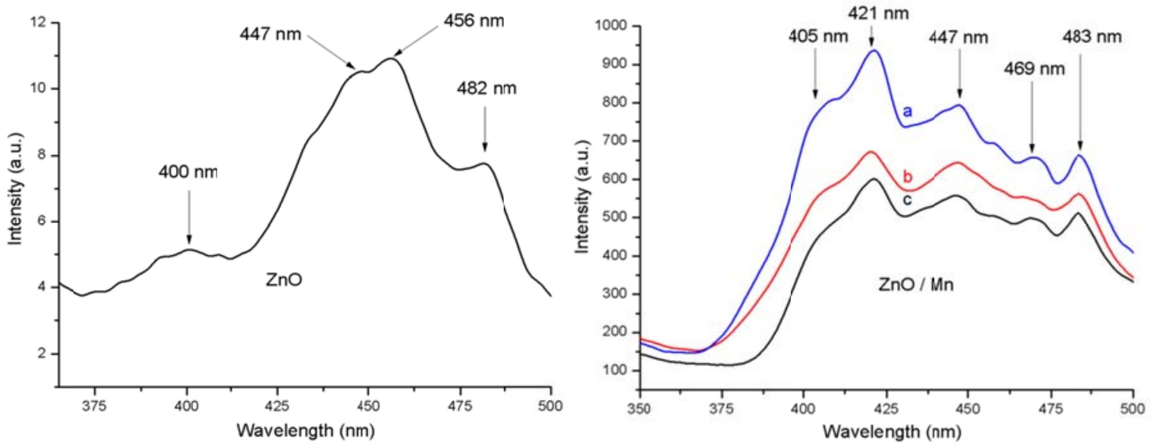

Fig. 4. Photoluminescence spectra of pure ZnO powder (left) and Mn-doped ZnO powder (right) samples at different doping levels (a) 1%, (b) 2.5% and (c) 5%

High intensity of the visible luminescence versus NBE are reported in literature whenever the luminescence spectra is recorded on powders as obtained, without further treatments (simple annealing or annealing in presence of reducing atmosphere) [29, 30].

It has been reported that the sub-band-gap emission in ZnO depends on the morphology of the nanostructures. [31-33]. A blue-green emission at 453 nm is found in literature for nest like nanoparticles [32] and emissions at 421 nm, 482 nm, and 532 nm for nanocones [33].

The results, figure 4, show that the as-synthesized samples have a wurtzite structure, with a weaker UV emission, and two blue-green emissions, one centred at 456 nm (with a shoulder at 447 nm) and a second at 482 nm. The weak UV emission at 400 nm is assigned to the free exciton emission from the wide band gap of ZnO (NBE). This peak is shifted to 405 nm upon increasing the dopant percentage. The shift in the band edge position is suggested to be caused byMn impurities introducing an impurity level in the band gap of ZnO [34].

The PL spectrum also exhibits two additional weak peaks at 2.95 eV (421 nm) and 2.56 eV (483 nm). These PL signals are attributed to band-edge free excitons and bound excitons, respectively [35].

The increase in the Mn(II) ions percentage has a direct effect on the intensity of the blue and violet emission. The decrease in intensity takes place systematically, which confirms the occurrence of doping dependence on the intensity. According to literatures, the quenching of the blue emission is caused by the apparition of electron capture centres on the surface of nanocrystals or the existence of nonradiative decay channels [36, 37]. This behaviour can be correlated with the insertion of Mn(II) ions on the surface of the nanoparticles. The intensity of the visible emission peak also correlates with the particle size [38] and shape [39].

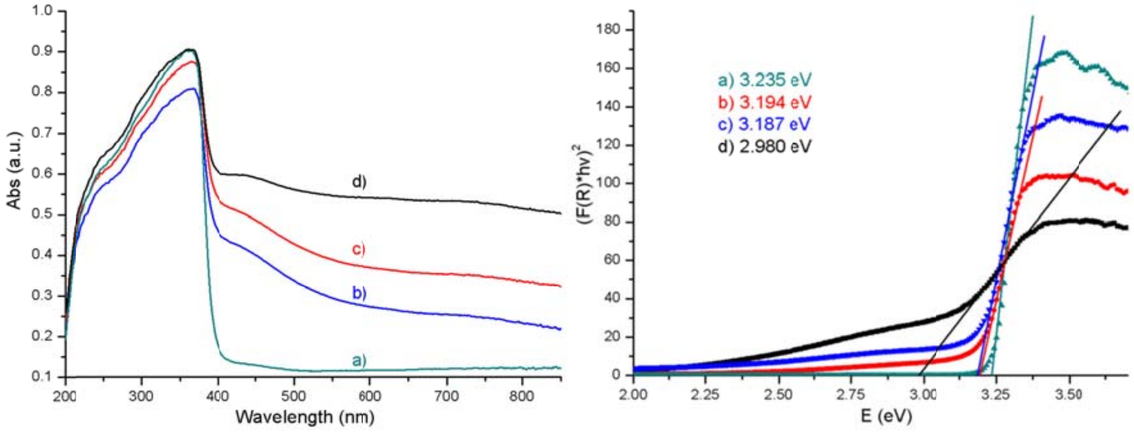

A B

Fig. 5. Diffuse reflectance spectra (A) and plot of the transformed Kubelka-Munk function vs. the energy (B) for the Mn-doped ZnO powder samples at different doping levels a) 0%; b) 1%; c) 2.5%; d) 5%.

The electronic spectra recorded for Mn-doped ZnO powder samples are presented in figure 5a. As it was expected, the introduction of the Mn ions in the lattice of ZnO has increased the absorbance of the nanopowder in the visible region of the spectrum. While ZnO is almost transparent to visible light, the sample doped with 5% Mn has a 60% absorption in the visible region.

The fundamental absorption refers to the optical transition of electrons from the valence band to conduction band and can be used to determine the nature and values of optical band gap of the nanoparticles [40, 41]. For analysis purposes the diffuse reflectance, *R*, of the sample can be related to the Kubelka-Munk function *F(R)* by the relation $F(R)=(1-R)^2/2R$, [42]. To determine the band-gap energies (Eg) for the Mn-doped ZnO powder samples, a plot of the square of the modified Kubelka-Munk function vs. the energy is presented in the figure 5b. This yields the direct band gap energy. Adopting the method proposed by Cao et al.,[43] the band-gap energies (Eg) for the Mn-doped ZnO powder samples are determined to be 3.13 eV, by the extrapolation to $[F(R)\cdot h\nu]^2 = 0$. The calculated band gap for the Mn-doped ZnO powder samples is smaller than that for pure ZnO, which is in good agreement with the fact that doping ions will introduce new electronic levels inside the ZnO band gap.

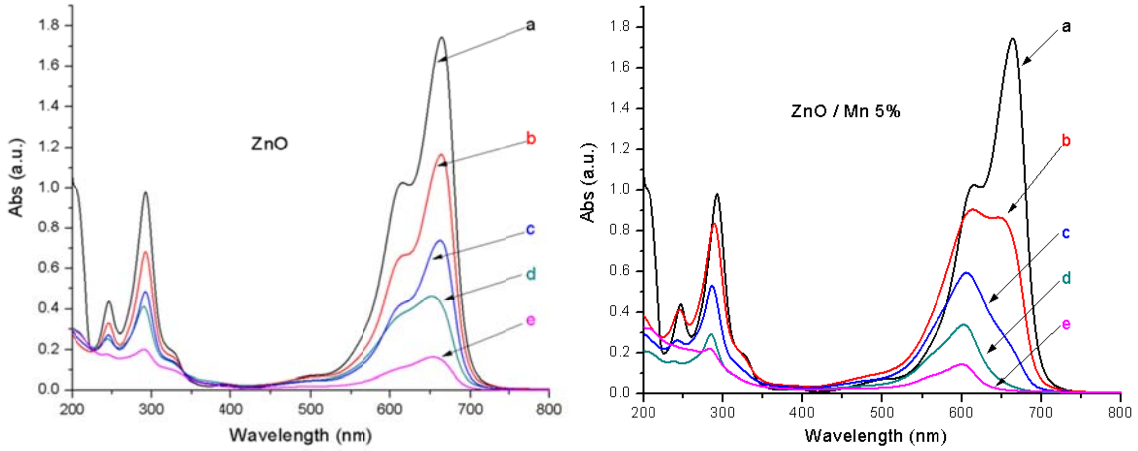

Fig. 6. Determination of photocatalytic activity of pure ZnO powder (left) and 5% Mn-doped ZnO powder (right) samples versus methylene blue: a) initial; b) after 60 min; c) after 120 min; d) after 180 min; e) after 240 min.

Like many thiazine dyes, MB has a tendency to dimerise. The dimer of MB, (MB)2, has an absorption maximum at 614 nm [44] vs 662 nm for the monomer MB [45].

The decreases of both absorption maximums, figure 6, indicate that all samples have a photocatalytic activity. Nevertheless, the degradation pathway of MB is different for pure ZnO and Mn–doped ZnO.

While in the case of ZnO sample, both MB and $(MB)_2$ maximums are decreasing at the same rate, in the case of Mn doped ZnO, the MB absorption maximum falls abruptly, while the $(MB)_2$ maximum decrease at a slower rate than in the case of ZnO. This indicates a rapid degradation of MB in the presence of Mn-doped ZnO, part of it being transformed in the dimer $(MB)_2$. The dimer is also degraded, after 4h of irradiation, the sample with Mn-doped ZnO containing slightly more $(MB)_2$ than the sample with ZnO, but no MB.

Because of the dimerization, the size of the molecule increases, this having a direct influence on photocatalysis process, through diffusion step. The decrease of the absorption maximum at 614 nm indicates that the Mn-doped ZnO possesses a photonic efficiency for degradation [46].

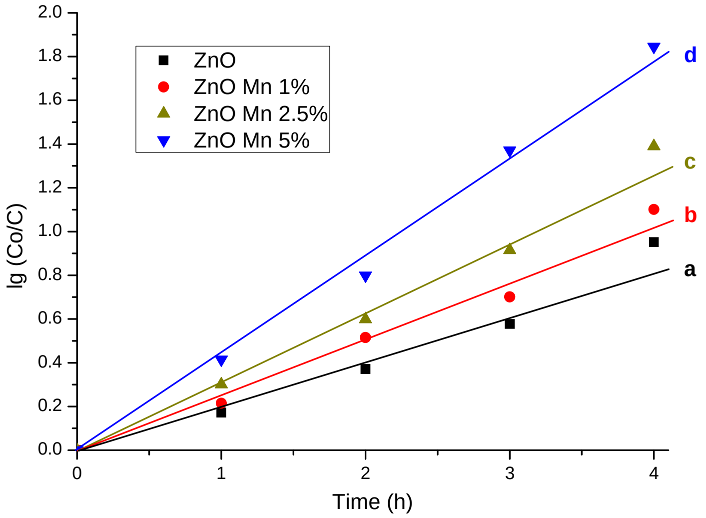

Fig. 7. Comparative evolution of lg(C_0/C) vs irradiation time

The study shows that although both samples (pure and doped ZnO) have photocatalytic activity, the mechanism is different. While ZnO equally degrades MB and $(MB)_2$, the doped Mn-ZnO transforms MB to $(MB)_2$ and afterwards strongly degrades the dimer. Overall, the Mn-doped samples have a better photocatalytic activity than pure ZnO, figure 7.

4. Conclusions

A synthetic method for the pure ZnO and Mn-doped ZnO nanocrystalline powder using non-basic hydrolysis has been presented. The forced hydrolysis produces a nanopowder that once dried at 120°C, contains ZnO, with no detectable secondary phases. The Mn ions were homogenously incorporated in the ZnO lattice, XRD analysis indicating existence of a single-phase compound, wurtzite. TEM and XRD data sustain the formation of a single phase, monodisperse crystalline Mn-doped ZnO nanopowder.

The band gap value of doped samples is smaller than the band gap value of the bulk ZnO, and it is decreasing with as the Mn dopant percent increases.

On UV excitation with 320nm the doped samples exhibited an overall diminished emission, the blue-green photoluminescence being much stronger than the excitonic one.

Also with increasing of Mn percent, we notice an increase in the photocatalytic activity.

Both effects, the quenched luminescence and better photocatalytic activity can be explained by an increasing in the surface defects associated with lattice distortion induced by Mn ions.

Acknowledgments

Authors recognize financial support from the European Social Fund through POSDRU/89/1.5/S/54785 project: "Postdoctoral Program for Advanced Research in the field of nanomaterials"

References

[1] C.I. Covaliu, T. Mălăeru, G. Georgescu, O. Oprea, L. Alexandrescu, I. Jitaru , Dig J Nanomater Bios., **6**(4), 1491 (2011)
[2] D. Ficai, A. Ficai, B. S. Vasile, M. Ficai, O. Oprea, C. Guran, E. Andronescu, Dig J Nanomater Bios., **6**(3), 943 (2011)
[3] C.I. Covaliu, L. C. Chioaru, L. Crăciun, O. Oprea, I. Jitaru Optoelectron. Adv. Mater. – Rapid Commun. **5**(10), 1097 (2011)
[4] A. Ianculescu, F. Prihor Gheorghiu, P. Postolache, O. Oprea, L.Mitoseriu, Journal of Alloys and Compounds **504**(2), 420 (2010)
[5] K.S. Weißenrieder, Muller - J. Thin Solid Films, **300** 30 (1997)
[6] H. Masai, T. Toda, T. Ueno, Y. Takahashi, T. Fujiwara - Appl. Phys. Lett., **94** 151908 (2009)
[7] M. A. Behnajady, N. Modirshahla, E. Ghazalian - Dig J Nanomater Bios. **6**(1), 467 (2011)
[8] C. Lorenz, A. Emmerling, J. Fricke, T. Schmidt, M. Hilgendorff, L. Spanhel, G. Muller, J. Non-Cryst. Solids, **238,** 1 (1998)
[9] A. Radu, S. Iftimie, V. Ghenescu, C. Besleaga, V.A. Antohe, G. Bratina, L. Ion, S. Craciun, M. Girtan, S. Antohe - Dig J Nanomater Bios. **6**(3), 1141 (2011)
[10] A. Gupta, H.S. Bhatti, D. Kumar, N.K. Verma, R.P. Tandon - Dig J Nanomater Bios. **1**(1), 1 (2006)
[11] F. Vaja (Dumitru), D. Ficai, A. Ficai, O. Oprea, C. Guran, J. Optoelectron. Adv. Mater **15**(1- 2), 107 (2013)
[12] Horng-Huey Ko, Hui-Ting Chen, Feng-Ling Yen, Wan-Chen Lu, Chih-Wei Kuo, Moo-Chin Wang - Int. J. Mol. Sci. **13**, 1658 (2012)
[13] Chao Hua Xue, Wei Yin, Shun Tian Jia, Jian Zhong Ma- Eco-Dyeing, Finishing and Green Chemistry **441**, 351 (2012)
[14] F. Vaja (Dumitru), C. Comanescu, O. Oprea, D. Ficai, C. Guran - Revista de Chimie **63**(7), 722 (2012)
[15] A. A. Dakhel, M. El-Hilo - Journal of Applied Physics **107**, 123905 (2010)
[16] L. Ion, S. Antohe, A. Sima, M. Sima - Dig J Nanomater Bios. **6**(4), 1695 (2011)
[17] F.I. Ezema, U.O.A. Nwankwo - Dig J Nanomater Bios. **6**(1), 271 (2011)
[18] O. Oprea, O. R. Vasile, G. Voicu, L. Craciun, E. Andronescu - Dig J Nanomater Bios. **7**(4), 1757 (2012)
[19] M.A. Mahmood, S. Baruah, J. Dutta - Materials Chemistry and Physics, **130**(1-2), 531 (2011)
[20] T. Tsuzuki, R.L. He, J.F. Wang, L. Sun, X.G. Wang, R. Hocking – International Journal of Nanotechnology, **9**(10-12), 1017 (2012)
[21] O. Oprea, E. Andronescu, B.S. Vasile, G. Voicu, C. Covaliu, Dig J Nanomater Bios. **6**(3)**,** 1393 (2011)
[22] O Oprea, O. R. Vasile, G. Voicu, L. Craciun, E. Andronescu - Dig J Nanomater Bios. **7**(4), 1757 (2012)
[23] O.R. Vasile, E. Andronescu, C. Ghitulica, B.S. Vasile, O. Oprea, E. Vasile, R. Trusca, Journal of Nanoparticle Research, **14**(12), art. no. 1269, (2012)
[24] O Oprea, O. R. Vasile, G. Voicu, E. Andronescu - Dig J Nanomater Bios. – **8**(2), in press (2013)

[25] A.F. Kohan, G. Ceder, D. Morgan, Chris G. Van de Walle - Phys. Rev. B. **61,** 15019 (2000)
[26] A. A. Dakhel, M. El-Hilo - Journal of Applied Physics **107,** 123905 (2010)
[27] Z.R. Tian, J.A. Voigt, J. Liu, B. Mckenzie, M.J. Mcdermott, M.A. Rodriguez, H. Konishi, H.F. Xu - Nat. Mater. **2,** 821 (2003)
[28] M.H. Huang, Y. Wu, H. Feick, N. Tran, E. Weber, P. Yang - Adv. Mater. **13,** 113 (2001)
[29] J.W.P. Hsu, D.R. Tallant, R.L. Simpson, N.A. Missert, R.G. Copeland, Applied Physics Letters **88,** 252103 (2006)
[30] Sh.U. Yuldashev, Sung Woo Choi, Tae Won Kang - Journal of the Korean Physical Society **42**, S216_S218 (2003)
[31] W.M. Kwok, A.B. Djurisic, Y.H. Leung, W.K. Chan, D.L. Phillips - Appl. Phys. Lett. **87**, 223111 (2005)
[32] Li Yan, Feng Hui-yun, Zhang Nan, Liu Chuan-sheng - Trans. Nonferrous Met. Soc. China **20**, 119 (2010)
[33] D.H. Zhang, Q.P. Wang, Z.Y. Xue - Appl. Surf. Sci. **207,** 20 (2003)
[34] Z. Wang, X. Y. Ma, J. W. Song, and J. H. Yao - Nano-Micro Letters, **1**(1), 45 (2009)
[35] J. Liqianga, Q. Yichuna, W. Baiqia, L. Shudana, J. Baojianga, Y. Libina, F. Weia, F. Honggang, S. Jiazhong - Sol. Energy Mater. Sol. Cells **90,** 1773 (2006)
[36] Y. Zhang, Y.D. Li - J. Phys. Chem. B **108,** 17805 (2004)
[37] Liu Wentan Ren, Yong Zhang, Yin-Xi Zhang - European Polymer Journal **47,** 1135 (2011).
[38] M. Wang, Na E K, J.S. Kim, E.J. Kim, S.H. Hahn, C. Park, K.K. Koo - Mater. Lett. **61**, 4094 (2007)
[39] A.Marcu, I.Enculescu, S.Vizireanu, R.Birjega, C.Porosnicu - Dig J Nanomater Bios. **8**(2), 597 (2013).
[40] S.M. Rozati, E. Shadmani - Dig J Nanomater Bios. **6**(2), 365 (2011)
[41] S. Singh, H. Kaur, D. Pathak, R.K. Bedi - Dig J Nanomater Bios. **6**(2), 689 (2011)
[42] Kortum, G. - Reflectance Spectroscopy; (1969) Springer-Verlag: New York
[43] G. Cao, L.K. Rabenberg, C.M. Nunn, T.E. Mallouk - Chem. Mater. **3,** 149 (1991)
[44] A. Mills, J. Wang - J. Photochem. And Photobiol. A: Chemistry **127,** 123 (1999)
[45] ISO/DIS 10678: Fine ceramics (advanced ceramics, advanced technical ceramics): Determination of photocatalytic activity of surfaces in an aqueous medium by degradation of methylene blue, standard under development
[46] Eva S. Lončar, Miroslava M. Radeka, Snežana B. Petrović, Andrea S. Skapin, Ognjen Lj. Rudić, Jonjaua G. Ranogajec Acta periodica technologica **40**, 125 (2009)